Geophysical Research Letters

RESEARCH LETTER
10.1029/2024GL108922

Complex Martinique Intermediate-Depth Earthquake Reactivates Early Atlantic Break-Up Structures

Mike Lindner[1], Andreas Rietbrock[1], Lidong Bie[2], Ya-Jian Gao[1], Saskia Goes[3], and Michael Frietsch[1]

[1]Karlsruhe Institute of Technology, Geophysical Institute, Karlsruhe, Germany, [2]University of East Anglia, School of Environmental Sciences, Norwich, UK, [3]Imperial College, London, UK

Abstract Earthquakes that rupture several faults occur frequently within the shallow lithosphere but are rarely observed for intermediate-depth events (70–300 km). On 29 November 2007, the M_w7.4 Martinique earthquake struck the Lesser Antilles Island Arc near the deep end of the Wadati-Benioff-Zone. The sparse regional seismic network of 2007 previously hampered a detailed examination of this unusually complex event. Here, we combine seismic data from different studies with regional moment tensor inversion results and 3D full-waveform modeling. We show that the earthquake is a doublet consisting of dip-slip and strike-slip motion along two oblique structures, both activated under extensional stress along the strike of the slab. Comparison with tectonic reconstructions suggests that the earthquake ruptured along a re-activated ridge-transform segment of the subducted Proto-Caribbean spreading ridge. The unprecedented resolution of the source process highlights the influence of pre-existing structures on localizing slab deformation also at intermediate-depth.

Plain Language Summary Some earthquakes in continents and near the ocean floor are known to break multiple, differently oriented, faults. Such compound earthquakes are rarely observed in subducted plates in the intermediate-depth region between 70 and 300 km. Intermediate-depth earthquake mechanics and stress state are possibly different from shallower earthquakes, and maybe they hinder complex events. On 29 November 2007, the M_w7.4 Martinique earthquake occurred at a depth of ∼150 km, near the deep end of the regional seismic zone below the Lesser Antilles Arc. The regional seismic network in 2007 was relatively sparse; it revealed the earthquake had a complex mechanism but did not previously allow for an in-depth study. In this study, we combine different types of data and methods, including full waveform information, based on a recently derived 3D regional velocity model. Our analyses shows that the Martinique earthquake consisted of at least two distinct sub-events on perpendicular faults in the subducted plate—a source doublet. By comparing the orientations of the doublet faults with plate tectonic reconstructions, we infer that this intermediate-depth earthquake broke along a fossil plate-boundary. This indicates that such structures remain structural weaknesses even after subduction.

Key Points:

- Moment tensor solutions, aftershock activity, back-projection, and source-time function suggest a complex rupture of the 29 November 2007, M_w7.4 Martinique earthquake
- Regional Moment Tensor modeling and aftershock cross-correlation identified the event as a source doublet
- Earthquake likely re-activated a fossil ridge-transform structure associated with the subducted Proto-Caribbean spreading ridge

Supporting Information:

Supporting Information may be found in the online version of this article.

Correspondence to:

M. Lindner,
mike.lindner@kit.edu

Citation:

Lindner, M., Rietbrock, A., Bie, L., Gao, Y.-J., Goes, S., & Frietsch, M. (2024). Complex Martinique intermediate-depth earthquake reactivates early Atlantic break-up structures. *Geophysical Research Letters*, *51*, e2024GL108922. https://doi.org/10.1029/2024GL108922

Received 27 FEB 2024
Accepted 17 MAY 2024

Author Contributions:

Conceptualization: Mike Lindner
Data curation: Mike Lindner
Formal analysis: Mike Lindner, Lidong Bie, Michael Frietsch
Funding acquisition: Andreas Rietbrock
Investigation: Mike Lindner, Andreas Rietbrock, Saskia Goes
Methodology: Mike Lindner, Ya-Jian Gao
Project administration: Andreas Rietbrock
Resources: Mike Lindner
Software: Mike Lindner, Ya-Jian Gao, Michael Frietsch
Supervision: Andreas Rietbrock

1. Introduction

Seismicity in the intermediate-depth range (70–300 km, Gutenberg & Richter, 1954) is prevalent in all large subduction zones (Astiz et al., 1988) and can be associated with intra-slab deformation of subducted lithosphere (Wadati, 1928). Yet the underlying physical mechanism is still debated (e.g., Green & Houston, 1995; Hobbs & Ord, 1988; Kelemen & Hirth, 2007; Kirby et al., 1990). Conventional mechanisms for shallow crustal earthquakes do not hold for the Wadati-Benioff seismicity (Green & Houston, 1995). The leading hypothesis is that intermediate-depth seismicity is caused/triggered by dehydration of hydrous minerals, leading either to dehydration embrittlement (Kirby et al., 1990), or to run-away plastic instabilities (Hobbs & Ord, 1988). Either way, these processes are governed by the breakdown of hydrous minerals in the slab (Green & Houston, 1995) that are likely more concentrated where fluids percolated into pre-existing faults created in the oceanic plate before its subduction (Hacker et al., 2003) or during bending at the trench (Ranero et al., 2005). Hence it has been proposed that intermediate-depth events re-activate such subducted fluid-rich structures (Garth & Rietbrock, 2014; Green & Houston, 1995; Warren et al., 2015). The driving force for intermediate-depth events are stresses due to gravitational pull, distortions of the slab in response to variations in slab buoyancy, slab unbending and the increasing resistance to sinking and/or decreasing space with depth (Astiz et al., 1988; Engdahl & Scholz, 1977; Isacks & Molnar, 1971; Warren et al., 2015).

Validation: Mike Lindner
Visualization: Mike Lindner
Writing – original draft: Mike Lindner
Writing – review & editing: Mike Lindner, Andreas Rietbrock, Lidong Bie, Ya-Jian Gao, Saskia Goes

Complex deformation may be reflected in earthquake rupture complexity, for example, leading to source doublets, seismic events that display different deformation styles on two temporally and spatially separated fault planes. Identifying source complexity for intermediate or deep earthquakes from aftershocks is challenging as the average aftershock-to-mainshock moment ratio is significantly lower than for similarly sized shallow events (Persh & Houston, 2004). Observations of such events are rare and may demand challenging modeling of the source process. Using back-projection, Kiser et al. (2011) analyzed 22 globally distributed intermediate-depth earthquakes for multiple subevents across several preexisting faults on the slabs. Other doublet observations of prominent earthquakes within the intermediate-depth include the 2015 M6.3 Bucaramanga earthquake (Poli et al., 2016), the 2015 M_w7.5 HinduKush earthquake (e.g., Zhan & Kanamori, 2016) or the even deeper 2018 M_w8.2 and 7.9 Fiji earthquakes (Jia et al., 2020).

Indications of complexity can be found in the moment tensor (MT) solution. A Compensated Linear-Vector Dipole (CLVD, Knopoff & Randall, 1970) component to the MT can be understood as an indicator for issues in the underlying model assumptions. These include issues with the recording system (Lindner et al., 2022), imprecise source locations (e.g., Vavryčuk & Kühn, 2012), inaccuracies in the velocity model due to complex geology (e.g., Pham & Tkalcic, 2021) including local anisotropic rock fabrics (Li et al., 2018), seismic noise (Lindner et al., 2022) or the source model itself as deviations from a single point shear source (Frohlich, 1995). Using a statistical analysis of historical MT solutions of different catalogs, Rösler et al. (2023) showed that large non-double-couple contributions are more likely to be related to the source itself, especially for large events.

The 2007 M_w7.4 Martinique earthquake clearly stands out as having one of the most complex source mechanisms, evidenced by a high CLVD part, two different double-couple solutions, a high aftershock seismicity rate, and a twin-peak back-projection result (IRIS DMC, 2011a). This makes it an ideal test case for investigating in detail complex rupture behavior of intermediate depth seismicity. We will interpret our findings in relation to the tectonic regime and bring the Martinique earthquake into a global context.

2. Global Statistics of High |CLVD| Earthquakes

We evaluate the global occurrence of high |CLVD| earthquakes (since 2000, $M_w \geq 5.2$) for events listed in the USGS database (U.S. Geological Survey, 2022). We separate the database into three depth ranges, shallow (<70 km, $N = 28{,}376$ events), intermediate-depth ($70 - 300$ km, $N = 3{,}826$ events), and deep (>300 km, $N = 914$ events), and highlight events exceeding M_w7 and absolute |CLVD| of 40%/80% (Figure 1).

Very high |CLVD| (>80%) contributions are mainly found for smaller events ($M_w \leq 6.5$) (Figures 1b, 1e, and 1h). At depths above 10 km, the majority of these events are of volcanic origin and related to the 2014–2015 activity in Iceland (Rodríguez-Cardozo et al., 2021). Other high |CLVD| events at depths <50 km usually occur in regions of tectonic complexity, for example, mid-oceanic ridges where high |CLVD| might result from doublets at ridge-transform intersections. Higher |CLVD| earthquakes may cluster in certain depth ranges (e.g., around <50 km and <25 km for shallow $M_w \geq 7.0$ events), but difficult to conclusively resolve (Figure S1 in Supporting Information S1).

At intermediate/deep depths, where overall seismicity rates are lower, high |CLVD| events (>80%) occur, except for a small accumulation at ∼100 km (f), without notable pattern in both depth ranges. Events with $M_w \geq 7.0$ follow the general depth distribution of smaller events and are likely slightly increased below 500 km (Figures 1b and 1c with Figures 1e–1f, 1h–1i). Two deep large high |CLVD| events (yellow) are related to seismic activity in the Fiji-Tonga subduction zone (e.g., Jia et al., 2020).

At all depths, the events in the catalog have Gutenberg-Richter distributions with a similar slope (∼0.8 for events with $M_w \geq 5.2$). A normal distribution fit to the CLVD component has a similar standard deviation of around 24% at all depths, and possibly a systematic shift of the mean from slightly negative at shallow depths to slightly positive at large depths (Figures 1a, 1d, and 1g). Overall, there is little indication from the catalog that intermediate-depth and deep earthquakes are less complex than shallow earthquakes.

The 2007 M_w7.4 Martinique earthquake (magenta star) stands out in all three depth ranges as the only strong magnitude ($M_w \geq 7.0$) event with a |CLVD| greater than 80% (Lindner et al., 2019).

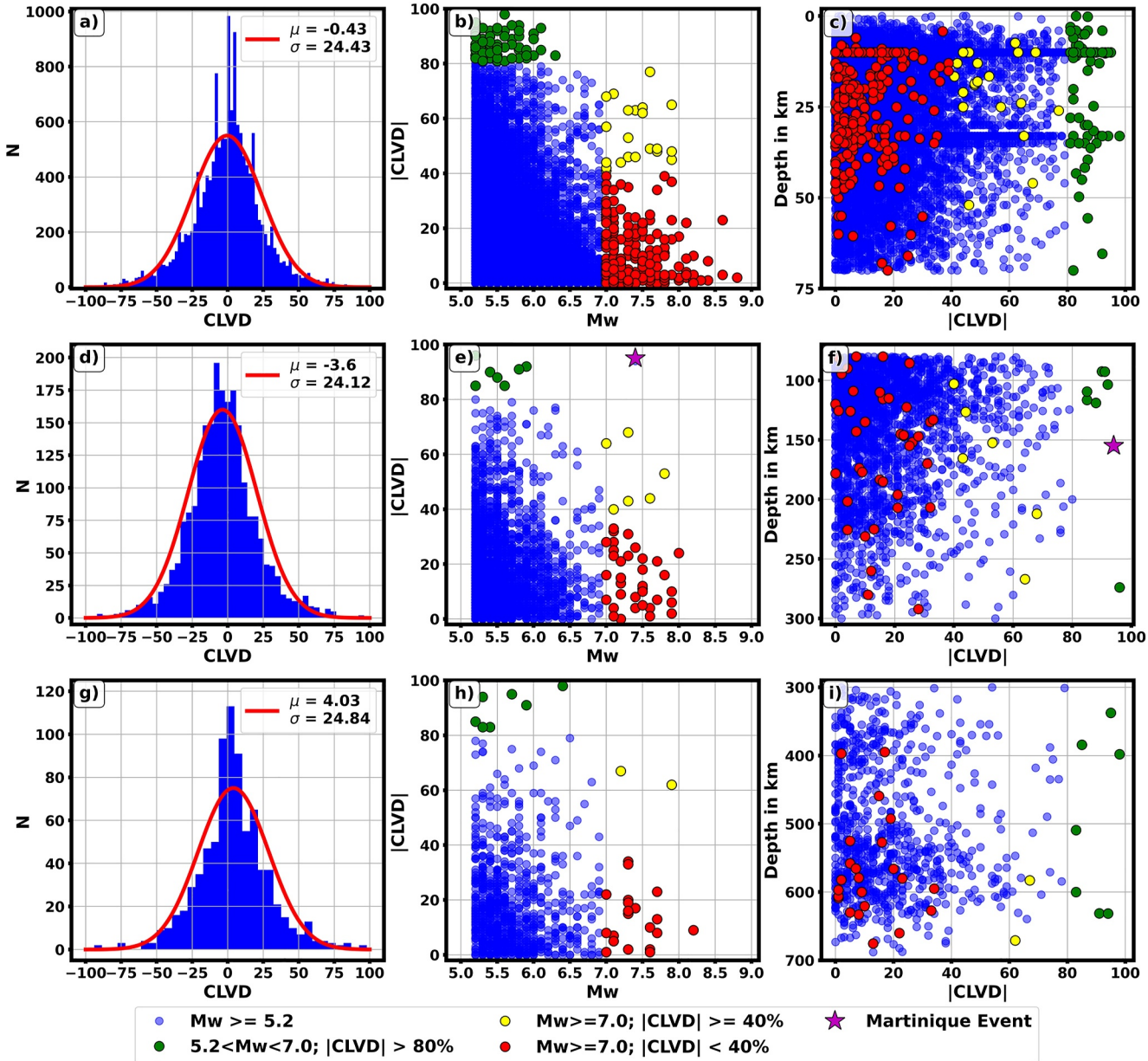

Figure 1. Global statistics of high |CLVD| earthquakes since 2000 with $M_w \geq 5.2$ in three depth ranges: (a)–(c) shallow (<70 km, $N = 28{,}376$), (d)–(f) intermediate-depth (70 − 300 km, $N = 3{,}826$), and (g)–(i) deep (>300 km, $N = 914$). The Compensated Linear-Vector Dipole components are fit with a normal distribution (a,d,g) which reveals a similar standard deviation σ but a depth-dependent mean μ. The events are grouped (b, e, h) according to their absolute |CLVD| and magnitude M_w with $5.2 < M_w < 7.0$ and |CLVD| > 80% in green, $M_w \geq 7.0$ and 40% ≤ |CLVD| > 80% in yellow, $M_w \geq 7.0$ and |CLVD| < 40% in red and remaining ones in blue. The absolute |CLVD| is plotted versus the source depth (c, f, i) to highlight potential depth dependencies.

3. The 2007 M_w7.4 Martinique Earthquake

The Martinique earthquake (Figure 2) is the largest instrumentally recorded seismic event in the Lesser Antilles Arc (LAA, e.g., Laigle et al., 2013; Hayes et al., 2017). Its automated IRIS back-projection solution (IRIS DMC, 2011a) shows two distinct energy peaks between Dominica and Martinique with a corresponding twin-peak source-time function (STF, Figure 2). Pre-existing deviatoric teleseismic MT solutions (Table S1 in Supporting Information S1, ev014) of different agencies have a strong CLVD component (>89%). The preferred USGS1 W-Phase solution reflects a dip-slip mechanism as underlying double-couple component, while the alternate USGS2 solution indicates a near strike-slip mechanism and so does the GCMT solution. Laigle et al. (2013) related the Martinique earthquake to possible heterogeneous slab structure (e.g., fossil fracture zone

10.1029/2024GL108922

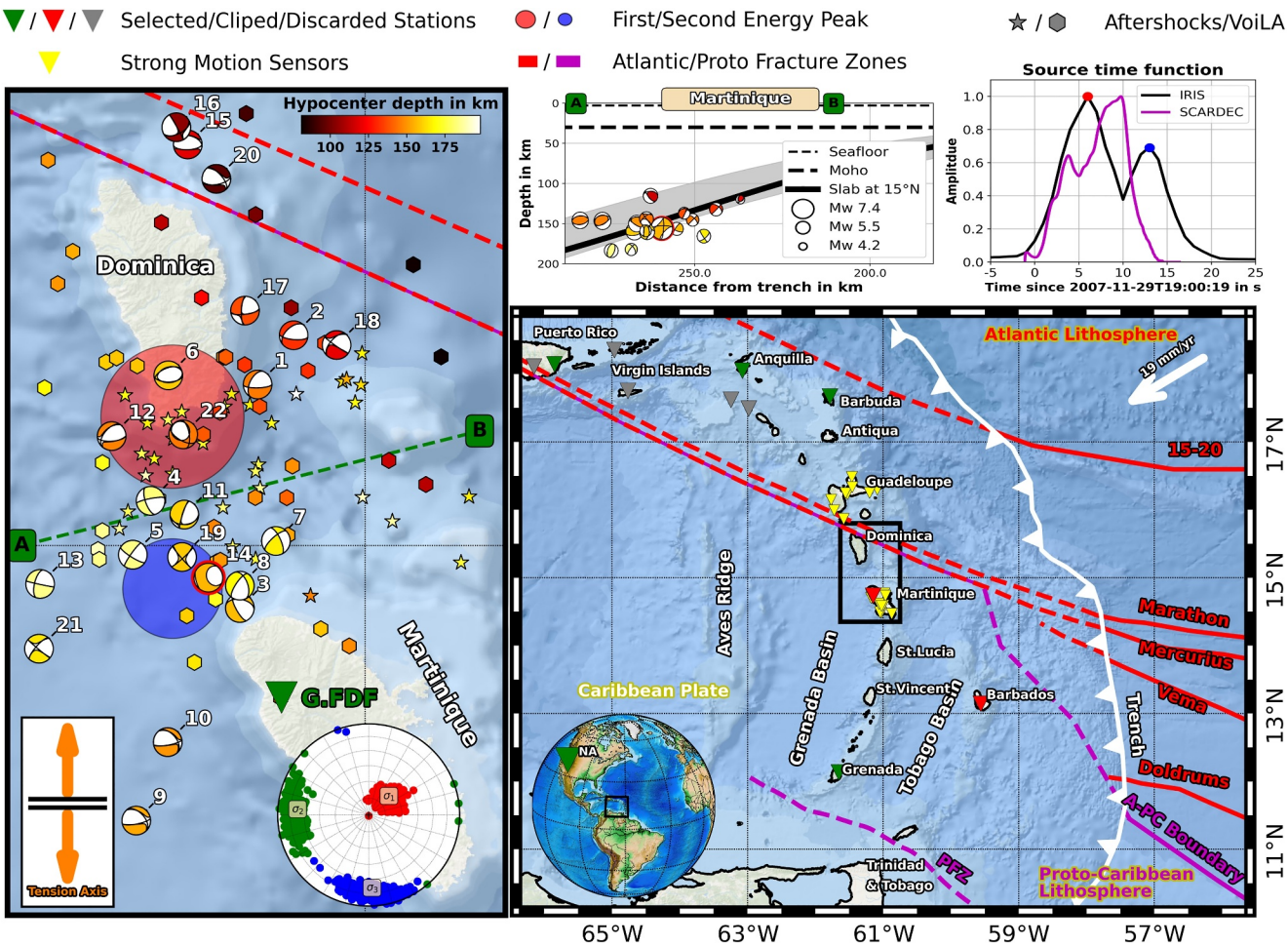

Figure 2. Bathymetric map of the Lesser Antilles subduction zone. Prominent FZs (solid before subduction, dashed projections after subduction) are marked in red on the Atlantic lithosphere, and magenta for inferred FZs of the Proto-Caribbean lithosphere. The trench is shown as white line, with plate motion relative to South America (Bie et al., 2020) along the white arrow. The domain boundary between the Atlantic and Proto-Caribbean lithosphere coincides with the Mercurius fracture zone at depth (red-magenta line). Triangles show the locations of the regional seismometer and strong motion network. The black box, embracing Dominica and Martinique, outlines the target area of this study. The IRIS back-projection (IRIS DMC, 2011a) results for the 2007 Martinique mainshock using data of the North-American seismic array (NA) show two distinct peaks in the source-time function and on the map (red/blue circle). Well-located seismic activity during the 2016 to 2017 VoiLA deployment (Bie et al., 2020) is depicted as stars and the IRIS recognized (IRIS DMC, 2011a) aftershocks are depicted as hexagons, all colored according to source depth. MTs for events around the 2007 Martinique earthquake from different publications (Table S1 in Supporting Information S1) are shown in the lower hemisphere projection and in a slab perpendicular cross-section view with ±75 km lateral slab extension (Lindner et al., 2022). The Martinique event is highlighted in the map view with a red circle around the beachball. The overall inferred extensional stress regime is depicted with the orange double arrow (Lindner et al., 2022).

(FZ) as previously proposed by Stein et al., 1982), however, did not recognize the ambiguity in the double-couple solutions and focused on the dip-slip mechanism.

The region between Dominica and Martinique exhibits the highest volcanic activity in the last 100k years (Wadge & Shepherd, 1984) and is thought to accommodate a gap in the slab causing anisotropic mantel flow (Schlaphorst et al., 2017). Seismicity in 120–180 km depth depicts a 40 km thick Wadati-Benioff-Zone (WBZ) and is associated with dehydration embrittlement (Bie et al., 2020). High Vp/Vs values are observed above the slab but reach also into it (Bie et al., 2022), while a seismic attenuation study (Hicks et al., 2023) found here the highest anomaly but noted the lack of spatial coincidence with the projected FZs north of Dominica. Recent studies concede the Mercurius FZ with the boundary between the Proto-Caribbean and Equatorial Atlantic oceanic domain (Braszus et al., 2021) and indicate the ancient spreading center perpendicular to it toward the south (Chen et al., 2024). Faulting activity at oceanic spreading centers shows a peculiar pattern of weakening structures that are re-activated under the present stress regime (Lindner et al., 2022).

3.1. Regional Stress Regime

Imaging of the subducted slab indicates a complex stress regime driven by substantial slab accumulation within the mantle transition zone and lateral variations in slab pull, which at the southern end of the LAA slab is reduced by partial detachment along a lateral slab tear below Grenada (Braszus et al., 2021). The slab deformation in response to the variations in slab pull appears to concentrate close to a segment of the extinct Proto-Caribbean ridge subducted below Martinique (Lindner et al., 2022). The overall inferred stress regime (using historical MTs, Figure 2) is trench-parallel extensional with (σ_1, σ_2, σ_3) = (54/71, 273/15, 180/11).

3.2. Historical Moment Tensor Solutions

We assembled a MT database of 22 events (Table S1 in Supporting Information S1), concentrated around the Martinique event (Dziewonski & Anderson, 1981; Ekström et al., 2012; Gonzalez et al., 2017; Lindner et al., 2022; Quinteros et al., 2021; U.S. Geological Survey, 2022) and observe a north-to-south change in faulting mechanisms (Figure 2). The northernmost events are normal events (e.g., ev020) with fault planes approximately parallel to the inferred trace of the subducted Marathon and Mercurius FZs. To the south, the fault planes of the normal faults are rotated (e.g., ev006), to near perpendicular to them. And at around 15°N, near the latitude of the Martinique event (red outline, ev014), the faulting style is predominantly strike-slip (e.g., ev005), including a dip-slip (ev011) and oblique thrust event (ev007). Finally, the southernmost events are again normal faults similar to those in the northernmost part, that is, with planes parallel to the FZ fabric.

3.3. Aftershocks

One foreshock and 32 aftershocks are associated with the Martinique earthquake, spanning a period of around six weeks (Table S2, Figure S3 in Supporting Information S1). One day prior to the main shock, an M_w3.7 event occurred ∼15 km away. Then, within 24 hr, 13 events were observed in its vicinity, increasing up to 19 events during the first week. The aftershock seismicity then faded, with a total number of 24 events accumulating within a month, of which only two events exceeded a magnitude of M_w5.0. Activity resurged after 37 days, with another sequence of 8 events (IRIS DMC, 2011a). This is unusual for intermediate-depth seismic events: about 48% of all intermediate-depth earthquakes with $M_w > 6.5$ have no and 37% only 1 to 5 recorded aftershocks (Astiz et al., 1988).

We performed a cross-correlation analysis to group the aftershocks (Figure S2 in Supporting Information S1). Due to sparse regional station coverage in 2007 and limited availability of data in the FDSN service, we are restricted to the vertical component of station FDF (Table S3 in Supporting Information S1) in the northern part of Martinique. Grouping is done using P- and S-wave information in a rather narrow bandpass between 1 and 2 Hz to counter path effects and the effect of differences in magnitude. P and S onsets are picked manually, using 5 s waveforms for P and 10 s for S. Cross-correlation coefficient matrices of P and S phases are calculated separately and rearranged per hand to identify groups that are common in both matrices or significant in only one of them. We selected several bridging events to join smaller subgroups together and could define two distinct groups. Group G1, shows large similarities in the P phase, exceeding 0.8, and a common pattern for S, using bridging events, at 0.65. In contrast, group G2 is more distinct in S and shows nearly no correlation in P.

Using the VoiLA earthquake database (Bie et al., 2020), we update the hypocenter locations for all ISC (IRIS DMC, 2011a) events including the aftershocks (Figure S4 in Supporting Information S1). The average source time update ($T_{0,\mathrm{Bie}} - T_{0,\mathrm{ISC}}$) is 1.35 ± 0.75 s and average location shift is [d_{lat}, d_{lon}, d_{depth}] = [−0.1125° ± 0.08°, 0.1303° ± 0.04°, 23.71 km ± 7.7 km]. This allows us to interpret the locations of both groups relative to the much better located moment tensors and larger geological structures (e.g., FZs).

Group G1 events (Figure 3, red) are focused to the north of 15°N, at an average depth of 145 km, while events of group G2 (blue) are located south of 15°N and vary in depth. The remaining events (black), which include the mainshock and the foreshock, occur primarily around 15°N, spatially separating groups G1 and G2. Associated with group G1 is the largest aftershock ev011 with M_w5.2. Its source mechanism has a similar double-couple component as the USGS1 solution of the mainshock and represents the faulting style of all events in its group. The GCMT double-couple component, being similar to the historical strike-slip events south of 15°N, might reflect the mechanisms of aftershock group G2. This suggests that the double-couple component of the USGS1 solution and the USGS2/GCMT solutions are close to the underlying mechanisms of the doublet.

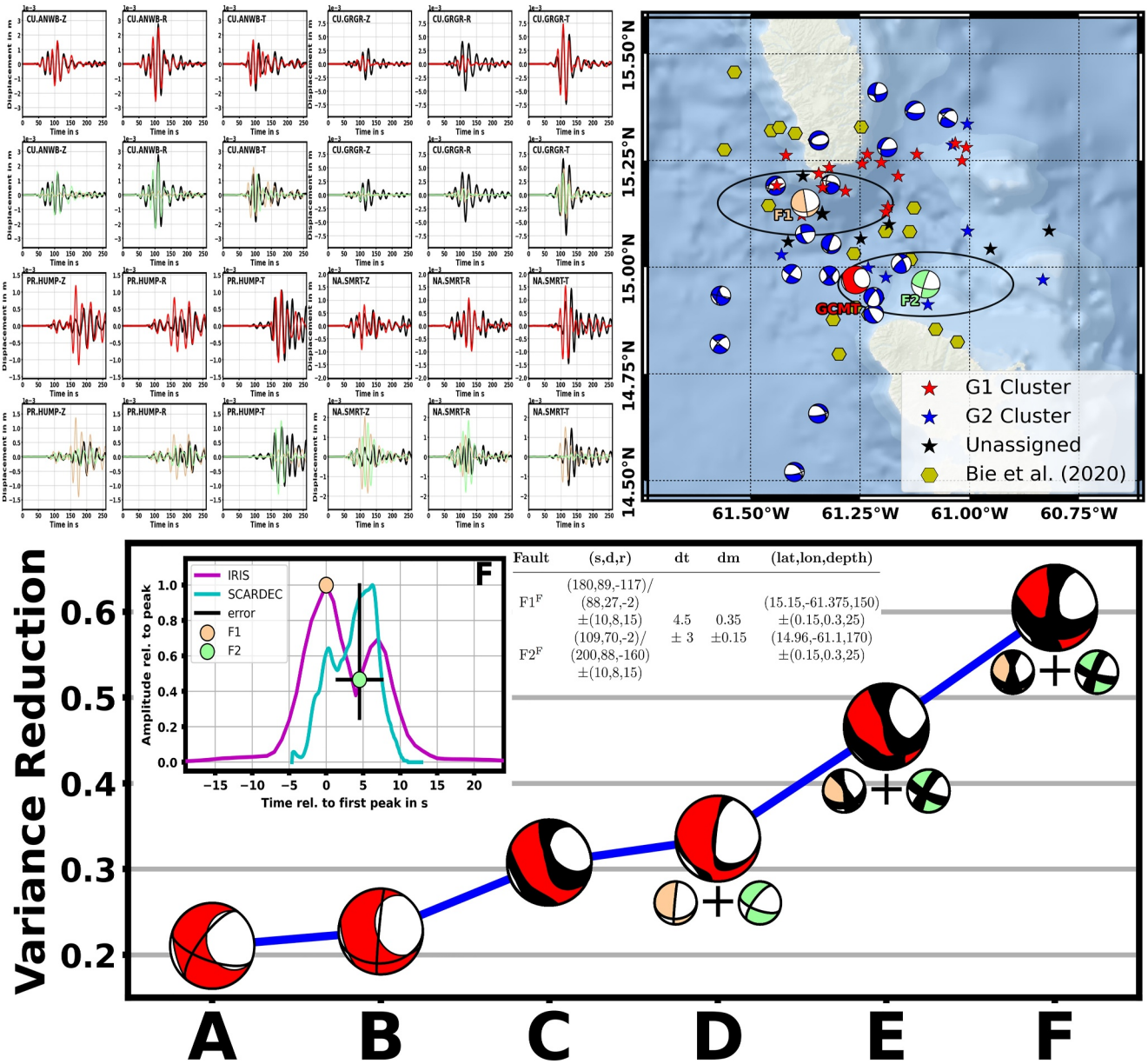

Figure 3. Regional 3D full waveform inversion. Displayed are our source models using a single fault (a)–(c) and doublet (d)–(f) assumption. Deviatoric beachballs (red) represent the weighted summation of the two double-couple mechanisms F1 (orange) and F2 (green). We performed forward simulations (a, b, d) and inversions (c, e, f) at fixed hypocenter locations (a)–(e) and in a location grid search (f). Inter-event-time *dt* is given relative to F1 (dip-slip, orange) and moment *dm* are fractions of the total released moment of M_w7.4. Displayed waveform fits are the results of experiment F in respective colors. The map gives an overview of the aftershock locations, locations of experiment F with uncertainty and the historical moment tensor solutions including the GCMT solution.

4. Source Modeling

To understand the contribution of the two sub-events (referenced as F1/F2), we perform regional moment tensor (RMT) modeling for the 2007 M_w7.4 earthquake and compare our results with local strong motion records and teleseismic data. Considering the limited network coverage at the time of the main event (Figure 2, Table S3 in Supporting Information S1), we expect discrepancies between the teleseismic solutions and our regional.

4.1. Data Selection

Seismometers on Martinique, MQ-Network and GEOSCOPE station FDF, are clipped and not useable for full-waveform source inversion. Toward the southeast, the HH-sensor on Barbados also clipped while the strong

motion HN-sensor recorded highly complex waveforms that cannot be explained by our velocity model. Strong motion records on Guadeloupe and Martinique of the RA-Network would provide additional data but are trimmed to 80 s and miss the full response information (gain factor). This left us with only one observation point south of the epicenter, Granada. Coverage in the north is slightly better but concentrates in northwestern direction; only three stations (Barbuda, Antigua, and Puerto Rico) are selected, to provide reasonable azimuthal coverage while avoiding over-representation of data in the north compared to the south. However, we use the strong-motion and teleseismic records to validate our solution.

4.2. Full Waveform Modeling

To improve the accuracy of the MTs, which are usually biased due to the inaccuracy of the regional velocity structure, we use the Spectral Element Method Salvus (Afanasiev et al., 2019) to simulate the Greens' Functions based on a regional 3D velocity model derived from teleseismic tomography (Braszus et al., 2021). We add the imaged isotropic V_P perturbations to the AK135 background model and assume the same perturbations (in %) to V_S. Surface and Moho topography were retrieved from crust1.0 (Laske et al., 2013). The spectral-element mesh is for an up to 3 s dominant period (12 km element size in the crust and 15–20 km in the upper mantle), to guarantee the accuracy of the numerical simulations. The simulations adopt a Heaviside STF.

4.3. Inversion Strategy

RMT modeling is done using an uniform importance sampling algorithm (AmΦB—uniXtree, Lindner et al., 2022). We conducted six experiment (Figure 3, Table S4 in Supporting Information S1), for single (a–c) and doublet fault (d–f) assumption, using forward simulations (a, b, d) to check existing solutions, and inversions (c, e, f) to get the best solutions with our database. The waveforms are bandpass filtered between 0.04 and 0.07 Hz (Figures S7–S12 in Supporting Information S1).

4.3.1. Single Fault

We conducted three single-source experiments: two forward simulations and one inversion. Issues with mismatches in timing are handled using a restricted cross-correlation time-shift update. We distinguish between uncertainties in the origin time and station delays by introducing a common 4 s time shift at all stations, and 6 s for the three-component waveforms at each station. This generous time update is conditioned by the limitations of the used P-wave travel-time velocity model (Braszus et al., 2021) which does not provide a sufficient resolution within our depth range and above and neglects the complex structure above the Martinique hypocenter (e.g., Hicks et al., 2023; Schlaphorst et al., 2017).

Forward simulations, of the GCMT (Figure 3a) and USGS (Figure 3b) solutions at a fixed hypocenter location, suggest a rather poor match between observations d and synthetics s, with a small variance reduction $\left(VR = 1 - NL2 = 1 - \frac{\|d-s\|}{\|d\|}\right)$ of 0.21 and 0.23, respectively. A subsequent deviatoric single fault inversion (Figure 3c) returns a slightly improved VR of 0.31, for a double-couple mechanism similar to the USGS1 solution. The inversion is done unbounded, where we allow an uniXtree importance sampling in full 4-dimensional parameter space: strike $\psi \in [0, 2\pi)$, dip $\delta \in \left[0, \frac{\pi}{2}\right]$ in the uniform Tape representation $h = \arccos(\delta)$ with $h \in [0, 1]$, rake $\lambda \in [-\pi, \pi)$ and CLVD $\in [-100\%, 100\%]$ in the uniform Tape representation $\gamma(v) = \frac{1}{3}\arcsin(3v)$ with $v \in \left[-\frac{1}{3}, \frac{1}{3}\right]$, $\gamma \in \left[-\frac{\pi}{6}, \frac{\pi}{6}\right]$ and CLVD $= \gamma \cdot \frac{600}{\pi}$ (Lindner et al., 2022). The main discrepancy of model C to model B is the strike direction, which we suggest to be a result of the network arrangement.

4.3.2. Doublet Fault

Doublet modeling follows the same procedure as for single fault cases but includes more parameters. We assume that the CLVD of a deviatoric singe fault solution can be explained by two appropriately temporally and spatially separated double-couple sub-events: a major and minor couple, each described by a set of strike, dip, and rake (Frohlich, 1995). The synthetic waveforms of both sub-events are simulated separately in a forward simulation and combined in a weighted summation of the time series. Sub-event succession in time is described by $dt \in [-15, 15]$, of F2 relative to F1. Negative times place F2 before, and positive times after F1. Magnitude differences are modeled using the moment ratio $dm \in [0.0, 1.0]$, relating to the total moment of the two sub-events. The amplitude of F2 is defined by dm, while the contribution of F1 is determined by $1 - dm$. Including the two hypocenter

locations, the doublet problem comprises 14 parameters: relative time *dt*, relative moment *dm*, two sets of three hypocenter location parameters and two sets of three fault-orientation parameters. This introduces large ambiguities in the solution if solved in the full parameter space. Therefore, we do a restricted inversion around a starting solution and/or fixed source locations.

Given that the GCMT/USGS solutions indicate two different mechanisms that agree with nearby historical mechanisms, we assume them to resemble the actual doublet. Our initial doublet test is composed of a combined forward simulation, with sampling of *dt* and *dm* (Figure S5 in Supporting Information S1), using the USGS1 double-couple as fault mechanism $F1^D$ and the GCMT double-couple as fault mechanism $F2^D$, at the USGS1 hypocenter location. The resulting doublet mechanism (Figure 3d) is strongly influenced by the $F1^D$ mechanism, $dm = 0.2$, and is followed by around 5.5 s by $F2^D$. However, the waveform fit increased only marginally compared to the single fault inversion to $VR = 0.34$. In the next step, we relax the constraints on fault mechanisms. Both couples are set as starting solutions in the restricted uniXtree-inversion (Lindner et al., 2022), allowing for a maximum deviation of d(strike, dip, rake) = (20°, 10°, 25°), together with the previous range for *dt* and *dm*. Resulting doublet (Figure 3e) has a smaller CLVD with $VR = 0.47$ and $dm = 0.34$. Offset time is 4.5 s, with $F1^E$ followed by $F2^E$. Finally, we solve for the spatial arrangement of the doublets $F1^F$ and $F2^F$ in a restricted uniXtree-inversion using a grid search. The location grid is constructed around the aftershocks (Figure S13 in Supporting Information S1) and informed by the re-located hypocenters (Bie et al., 2020). $F1^F$ is searched in the northern grid and $F2^F$ in the southern one. The inversion shows that the mechanisms of $F1^F$ and $F2^F$ do not change significantly; the spatial separation increases the waveform fit to $VR = 0.54$ (Figure 3f).

4.3.3. Validation

We use teleseismic (Figures S14–S16 in Supporting Information S1) and strong motion (Figures S17 and S18 in Supporting Information S1) recordings to validate our doublet solution. Teleseismic data are bandpass filtered between 150 and 275 s and compared with the GCMT and our solution. To counter differences in the regional to the PREM model, we computed the synthetics within the source parameter uncertainty. The overall fit supports our model whereas differences between both solutions can be explained by the vague information content of the GCMT-CLVD which is not fully described by a doublet but may also include higher complexities in the source/earth model. Strong motion data (0.1–0.175 Hz) depict variations in the strike of F1 and rake in F2 for stations in the north versus the south. However, these are within the given uncertainty and may reflect the influence of the local geology (Hicks et al., 2023; Schlaphorst et al., 2017) and/or the extended source. Lastly, we used regional first motion polarities to compare the inferred pattern to the two doublet solutions. The polarities show a better fit to a dip-slip mechanism, supporting the proposed timely succession (Table S5 and Figure S6 in Supporting Information S1).

5. Discussion

Our detailed MT inversion demonstrates that the Martinique earthquake was most likely a source doublet, consisting of two sequential sub-events in time and space: a M_w7.25 ± 0.05 dip-slip event followed, with a ∼4.5 ± 3.0 s delay, by a M_w7.15 ± 0.05 strike-slip event. Uncertainty in the inter-event time is possible larger due to the allowed time shifts. Using a scaling relationship for intra-slab earthquakes (Blaser et al., 2010), we can estimate the rupture length of the two sub-events, yielding ∼55 km each. The temporal/spatial succession is reversed relative to the SCARDEC-STF results but aligns well with the IRIS back-projection (Figure 3). Both mechanisms are consistent with the faulting pattern in the region and reconcile the discrepancy between the two published double-couple solutions. This leaves us with the question of which large(r) structure(s) at depth may have ruptured during this complex earthquake.

Seismicity at this depth represents intra-slab deformation (Bie et al., 2020; Lindner et al., 2022). Figure 4 displays our results relative to the slab surface. The background seismicity (heatmap, LAA ISC catalog since 1970) concentrates north of the Martinique event on the Proto-Caribbean lithosphere near the domain boundary to the Atlantic lithosphere. We made a qualitative assumption of the active nodal planes (preferred strike direction) of the events in our RMT catalog (white lines). The displayed pattern does not coincide with the Marathon-Mercurius FZs/domain boundary. Near this boundary, we observe some sub-parallel events, however, the faulting style then rotates, in a southward trend, to perpendicular and then approximately parallel to the FZ trend and finally perpendicular to it again.

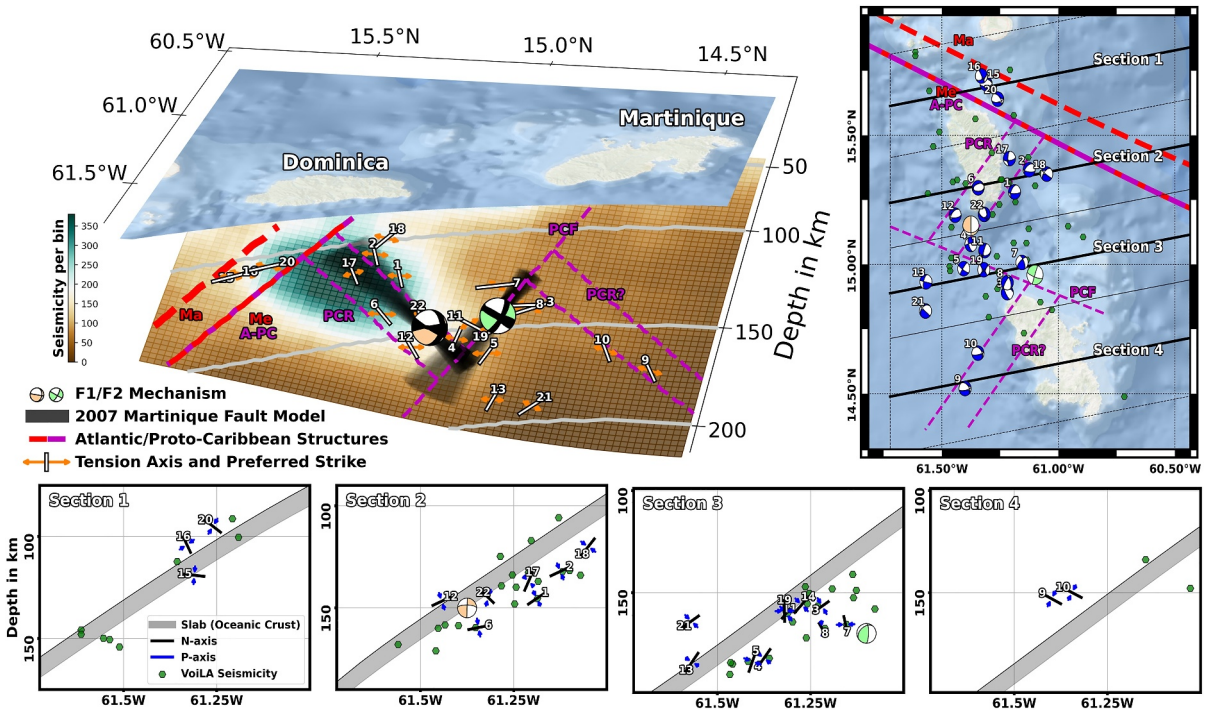

Figure 4. 3D sketch and depth cross-sections of the slab segment between Dominica and Martinique. Top: The Martinique earthquake is located at the proposed ancient ridge-transform intersection (magenta lines with unnamed fracture zone PCF and two offset ridge segments to the north PCR and south PCR?) on the Proto-Caribbean plate. Orientated perpendicular to the Atlantic-Proto-Caribbean domain boundary (A-PC), it got re-activated under the local trench parallel extension which probably accommodates the steepening of the slab from south to north (Lindner et al., 2022). Associated with A-PC are two Atlantic FZs: Mercurius (Me) which cannot be distinguished from the boundary at depth and Marathon (Ma). The outline of these structures is motivated by the source solutions and seismicity. Tension axes of known source mechanisms in the region are predominantly trench parallel and the nodal planes fit well to the suggested Proto-Caribbean structures. The Martinique doublet (F1/F2 mechanism) is located at the ridge-transform intersection, suggesting a rupture along these perpendicular structures. Both beachballs are in lower hemisphere projection. See also Figures S19–S23 in Supporting Information S1. Bottom: Trench perpendicular cross-sections showing the seismicity within the dotted boxes surrounding the profiles (map view). Sections 1 and 4 contain MTs with similar stress directions and seismicity overlaps with the estimated position and thickness of the subducted oceanic crust at depth. The middle sections host the highest seismic activity over a depth range significantly exceeding the expected thickness of the subducted oceanic crust. In both sections, mechanisms reflect along-strike extension and slab-perpendicular compression, but along Section 2 this stress is released mainly by normal fault events perpendicular to the A-PC while in Section 3 there is increased strike-slip activity.

Two recent studies (Braszus et al., 2021; Chen et al., 2024) predicted from the plate reconstruction by Müller et al. (2019) and comparison with tomography that the northernmost end of the ancient Proto-Caribbean spreading ridge subducted near the location of this deep earthquake cluster (R0 and Demerara FZ in Chen et al. (2024)). This part of the Proto-Caribbean ridge separated around 90 Ma ago from the Atlantic triple junction (North-Atlantic, Central-Atlantic and Proto-Caribbean), migrating westwards along the southern side of the Mercurius FZ and stopped spreading by ~50 Myr ago. The overall structure indicated by the nodal planes strongly resembles a ridge-transform fault system on oceanic lithosphere, with a spatial succession of dip-slip faulting on structures that are parallel to the subducted ridge segment PCR and strike-slip motion on faults parallel to the subducted FZ FCF (Figure 4).

The 2007 main doublet event occurs near where we observe a transition between these faulting styles, which is likely the location of a fossil ridge-transform intersection. Shallow-source doublet events, with large CLVD contributions when inverting for a single fault mechanism, have also been found to commonly occur near such fault intersections (Frohlich, 1995).

In a view along vertical cross-sections (Figure 4), we find along Section 1/4 that N-axes (null-axes) are near perpendicular and P-axes (pressure-axes) parallel to the down-dip direction of the slab, while T-axes are parallel to the slab strike. Events in these cross sections with MTs, as well as other events located using the regional stations and seismic structure (Bie et al., 2020), fall in an approximately 10 km wide band near the estimated position of the slab surface. The style of deformation and width of the WBZ in these two sections is similar to that found in other subduction zones, and reflects compression due to mantle resistance to slab sinking. The relatively

shallow occurrence of down-dip compression is consistent with the large amount of accumulated slab material within the upper mantle below the LAA as inferred from the tomographic images (Braszus et al., 2021). Section 2 hosts mostly normal faults with extension parallel to the trench, and N-axes parallel and P-axes perpendicular to the down-dip direction of the slab. Stress orientations are similar along Section 3, but with an increased number of strike-slip events and a mixture of N-axes parallel and perpendicular to the slab. The state of stress along Sections 2/3 is consistent with along-strike slab bending to accommodate the change in dip (Bie et al., 2020) between the steeper slab north and more shallow dipping slab south of Martinique.

As suggested by Lindner et al. (2022), such changes in dip could be due to partial slab detachment below Grenada. Changes in event style around the Martinique event thus does not reflect a change in stress, but solely a change in orientation of the ridge-transform inherited weak structures present in the slab that are activated in response to this stress. The seismicity in Sections 2/3, including the aftershocks, extends over a significantly larger depth range (20–30 km) below the inferred slab top location. Thickening of the WBZ near the Marathon FZ was reported (Bie et al., 2020). It could either reflect that the Martinique event and aftershocks ruptured deep into the slab, possibly due to deep hydration along the FZs/ridge structure (Braszus et al., 2021), or the WBZ may appear wide because of the superposition of events in two sections of the slab that are somewhat vertically offset due to along-strike folding or vertical motion along a tear to accommodate the dip change.

6. Conclusion

Our detailed study of the Martinique doublet together with recent tomography and reconstructions of this region which locate the subducted fossil Proto-Caribbean spreading ridge Braszus et al. (2021); Chen et al. (2024) provide probably the most conclusive evidence to date that intermediate-depth events can re-activate pre-existing distributed fault systems inherited from the creation of oceanic lithosphere. The re-activation below Martinique is governed by a predominant trench-parallel extensional stress regime (Lindner et al., 2022) and slab bending influenced by along-strike changes in slab pull due to partial slab detachment (Braszus et al., 2021; Lindner et al., 2022), which lead to local distortion of the slab and therefore facilitates the occurrence of large intermediate-depth earthquakes.

We showed that pre-existing structures facilitate the localization of seismic deformation even under high-pressure conditions in WBZ, for example, due to a concentration of hydration and/or weaker rheology because of inherited grainsize or fabric. It is possible that more pervasive hydration and faulting of the Atlantic lithosphere formed by slow spreading (Goes et al., 2019) makes these weaknesses more prominent than in fast-spread Pacific lithosphere, explaining the unusually high |CLVD| of the Martinique event. The potential of such earthquake doublets makes estimating maximum rupture sizes for intermediate-depth earthquakes challenging, but these possible locations could be mapped with high resolution plate reconstruction models.

Acronyms

USGS	United States Geological Service
IRIS	Incorporated Research Institutions for Seismology
GCMT	Global Centroid-Moment-Tensor
ISC	International Seismological Centre
MT	Moment Tensor
STF	Source-Time-Function
VR	Variance-Reduction
F1	Fault 1
F2	Fault 2
FZ	Fracture zone
A-PC	Atlantic Proto-Caribbean boundary

PCF	Proto-Caribbean Fracture zone
PCR	Proto-Caribbean ridge
PCR?	Possible Proto-Caribbean ridge
Me	Mercurius fracture zone
Ma	Marathon fracture zone
LAA	Lesser Antilles Arc
WBZ	Wadati-Benioff-Zone

Data Availability Statement

All data needed to evaluate the conclusions in the paper are provided in the paper and/or the Supporting Information. The stress inversion results are available in Lindner et al. (2022). Historical MT solutions are by Dziewonski and Anderson (1981); Ekström et al. (2012); Quinteros et al. (2021); U.S. Geological Survey (2022); Gonzalez et al. (2017); Lindner et al. (2022). Source-time function, backprojection results and aftershock list/locations were downloaded from IRIS DMC (2011b). The regional 3D velocity model is available in Braszus et al. (2021). Observed regional waveform data (network G by Institut de physique du globe de Paris (IPGP), and Ecole et Observatoire des Sciences de la Terre de Strasbourg (EOST) (1982), CU by Albuquerque Seismological Laboratory (ASL)/USGS (2006), IU by Albuquerque Seismological Laboratory/USGS (2014), PR by University of Puerto Rico (1986) and NA by KNMI (2006)), teleseismic waveform data (network G by Institut de physique du globe de Paris (IPGP), and Ecole et Observatoire des Sciences de la Terre de Strasbourg (EOST) (1982), II by Scripps Institution of Oceanography (1986), IU by Albuquerque Seismological Laboratory/USGS (2014) and MN by MedNet Project Partner Institutions (1990)) and strong motion waveform data (network RA by RESIF (1995)) were downloaded via obspy FSDN from the IRIS data management center. Seismometer data of the Martinique Seismic and Volcano Observatory Network (MQ network by Institut De Physique Du Globe De Paris (IPGP) (2020)) on Martinique are available upon request from the corresponding author or corresponding original distributor (see acknowledgments). Informations extracted from MQ data are polarities, which are listed in the Supporting Information. The free python software obspy by Beyreuther et al. (2010) was used for seismological data analysis and waveform download. The python package libcomcat by Libcomcat Developer Team (2022) was used to download the global MT database. Featured figures were created using the python package matplotlib/basemap by Hunter (2007); Caswell et al. (2020). Pyrocko by Heimann et al. (2017) was used to create the beachballs with polarity information. Salvus by Afanasiev et al. (2019) was used for the simulation of the 3D synthetic waveforms. PREM synthetic waveforms used for teleseismic validation are simulated using Instaseis by van Driel et al. (2015). The KIT in-house developed AmΦB—"Amphibious Bayesian" by Lindner et al. (2022) was used for RMT inversion and forward simulation. The analysis codes and related scripts for generating figures used in the main text and Supplement Information are available from the corresponding authors upon reasonable request.

Acknowledgments
This work was funded under Natural Environment Research Council Grant NE/K010611/1 and by the Geophysical Institute at KIT. We thank the data centers as well as the organizations that operate the seismic networks for kindly providing waveform data, MTs, back-projection product and aftershock list. In this context, we thank Alex Hutko of the Research Scientist at University of Washington for the E-Mail correspondence for the insight into the IRIS back-projection products. We thank Bertrand Delouis from the Geoazur for mediating data exchange of strong motion data on Guadeloupe and Martinique. We thank Valerie Clouard of the Géosciences Environnement Toulouse for mediating data exchange of seismometer stations on Martinique. Lastly, the authors gratefully acknowledge the Earth System Modelling Project (ESM) for supporting this work by providing computing time on the ESM partition of the supercomputer JUWELS (Alvarez, 2021) at the Jülich Supercomputing Centre. Open Access funding enabled and organized by Projekt DEAL.

References

Afanasiev, M., Boehm, C., Van Driel, M., Krischer, L., Rietmann, M., May, D. A., et al. (2019). Modular and flexible spectral-element waveform modelling in two and three dimensions [software]. *Geophysical Journal International*, *216*(3), 1675–1692. https://doi.org/10.1093/gji/ggy469

Albuquerque Seismological Laboratory (ASL)/USGS. (2006). Caribbean network [dataset]. *International Federation of Digital Seismograph Networks*. https://doi.org/10.7914/SN/CU

Albuquerque Seismological Laboratory/USGS. (2014). Global seismograph network (GSN – IRIS/USGS) [dataset]. *International Federation of Digital Seismograph Networks*. https://doi.org/10.7914/SN/IU

Alvarez, D. (2021). Juwels cluster and booster: Exascale pathfinder with modular supercomputing architecture at Juelich Supercomputing Centre. *Journal of Large-Scale Research Facilities*, *7*, A183. https://doi.org/10.17815/jlsrf-7-183

Astiz, L., Lay, T., & Kanamori, H. (1988). Large intermediate-depth earthquakes and the subduction process. *Physics of the Earth and Planetary Interiors*, *53*(1), 80–166. https://doi.org/10.1016/0031-9201(88)90138-0

Beyreuther, M., Barsch, R., Krischer, L., Megies, T., Behr, Y., & Wassermann, J. (2010). Obspy: A python toolbox for seismology [software]. *Seismological Research Letters*, *81*(3), 530–533. https://doi.org/10.1785/gssrl.81.3.530

Bie, L., Hicks, S., Rietbrock, A., Goes, S., Collier, J., Rychert, C., et al. (2022). Imaging slab-transported fluids and their deep dehydration from seismic velocity tomography in the Lesser Antilles subduction zone. *Earth and Planetary Science Letters*, *586*, 117535. https://doi.org/10.1016/j.epsl.2022.117535

Bie, L., Rietbrock, A., Hicks, S., Allen, R., Blundy, J., Clouard, V., et al. (2020). Along-arc heterogeneity in local seismicity across the Lesser Antilles subduction zone from a dense ocean-bottom seismometer network. *Seismological Research Letters*, *91*(1), 237–247. https://doi.org/10.1785/0220190147

Blaser, L., Krueger, F., Ohrnberger, M., & Scherbaum, F. (2010). Scaling relations of earthquake source parameter estimates with special focus on subduction environment. *Bulletin of the Seismological Society of America*, *100*(6), 2914–2926. https://doi.org/10.1785/0120100111

Braszus, B., Goes, S., Allen, R., Rietbrock, A., Collier, J., Harmon, N., et al. (2021). Subduction history of the Caribbean from upper-mantle seismic imaging and plate reconstruction. *Nature Communications*, *12*(1), 4211. https://doi.org/10.1038/s41467-021-24413-0

Caswell, T. A., Droettboom, M., Lee, A., Hunter, J., Firing, E., de Andrade, E. S., et al. (2020). matplotlib/matplotlib: Rel: v3.2.2. *Zenodo*. https://doi.org/10.5281/zenodo.3898017

Chen, Y.-W., Wu, J., & Goes, S. (2024). Lesser Antilles slab reconstruction reveals lateral slab transport under the Caribbean since 50 ma. *Earth and Planetary Science Letters*, *627*, 118561. https://doi.org/10.1016/j.epsl.2023.118561

Dziewonski, A. M., & Anderson, D. L. (1981). Preliminary reference earth model. *Physics of the Earth and Planetary Interiors*, *25*(4), 297–356. https://doi.org/10.1016/0031-9201(81)90046-7

Ekström, G., Nettles, M., & Dziewoński, A. (2012). The global CMT project 2004–2010: Centroid moment tensors for 13,017 earthquakes [Dataset]. *Physics of the Earth and Planetary Interiors*, *200–201*, 1–9. https://doi.org/10.1016/j.pepi.2012.04.002

Engdahl, E. R., & Scholz, C. H. (1977). A double Benioff zone beneath the central Aleutians: An unbending of the lithosphere. *Geophysical Research Letters*, *4*(10), 473–476. https://doi.org/10.1029/GL004i010p00473

Frohlich, C. (1995). Characteristics of well-determined non-double-couple earthquakes in the Harvard CMT catalog. *Physics of the Earth and Planetary Interiors*, *91*(4), 213–228. https://doi.org/10.1016/0031-9201(95)03031-Q

Garth, T., & Rietbrock, A. (2014). Order of magnitude increase in subducted H_2O due to hydrated normal faults within the Wadati-Benioff zone. *Geology*, *42*(3), 207–210. https://doi.org/10.1130/G34730.1

Goes, S., Collier, J., Blundy, J., Davidson, J., Harmon, N., Henstock, T., et al. (2019). Project voila: Volatile recycling in the Lesser Antilles. *Eos Transactions American Geophysical Union*, *100*. https://doi.org/10.1029/2019EO117309

Gonzalez, O., Clouard, V., & Zahradník, J. (2017). Moment tensor solutions along the central lesser Antilles using regional broadband stations. *Tectonophysics*, *717*, 214–225. https://doi.org/10.1016/j.tecto.2017.06.024

Green, H. W., & Houston, H. (1995). The mechanics of deep earthquakes. *Annual Review of Earth and Planetary Sciences*, *23*(1), 169–213. https://doi.org/10.1146/annurev.ea.23.050195.001125

Gutenberg, B., & Richter, C. (1954). *Seismicity of the earth and associated phenomena*. Princeton University Press. Retrieved from https://books.google.de/books?id=YOcKAQAAIAAJ

Hacker, B. R., Peacock, S. M., Abers, G. A., & Holloway, S. D. (2003). Subduction factory 2. Are intermediate-depth earthquakes in subducting slabs linked to metamorphic dehydration reactions? *Journal of Geophysical Research*, *108*(B1). https://doi.org/10.1029/2001JB001129

Hayes, G. P., Meyers, E. K., Dewey, J. W., Briggs, R. W., Earle, P. S., Benz, H. M., et al. (2017). *Tectonic summaries of magnitude 7 and greater earthquakes from 2000 to 2015*. U.S. Geological Survey Open-File Report 2016–1192. https://doi.org/10.3133/ofr20161192

Heimann, S., Kriegerowski, M., Isken, M. P., Cesca, S., Daout, S., Grigoli, F., et al. (2017). Pyrocko – An open-source seismology toolbox and library [software]. *GFZ Data Services*. https://doi.org/10.5880/GFZ.2.1.2017.001

Hicks, S., Bie, L., Rychert, C. A., Harmon, N., Goes, S., Rietbrock, A., et al. (2023). Slab to back-arc to arc: Fluid and melt pathways through the mantle wedge beneath the Lesser Antilles. *Science Advances*, *9*(5). https://doi.org/10.1126/sciadv.add2143

Hobbs, B. E., & Ord, A. (1988). Plastic instabilities: Implications for the origin of intermediate and deep focus earthquakes. *Journal of Geophysical Research*, *93*(B9), 10521–10540. https://doi.org/10.1029/JB093iB09p10521

Hunter, J. D. (2007). Matplotlib: A 2d graphics environment [software]. *Computing in Science & Engineering*, *9*(3), 90–95. https://doi.org/10.1109/MCSE.2007.55

Institut De Physique Du Globe De Paris (IPGP). (2020). Seismic, tiltmeter, groundwater, magnetic and weather permanent networks on Montagne Pelée volcano and Martinique [dataset]. Institut de physique du globe de Paris (IPGP), Université de Paris. https://doi.org/10.18715/martinique.mq

Institut de physique du globe de Paris (IPGP), and Ecole et Observatoire des Sciences de la Terre de Strasbourg (EOST). (1982). Geoscope, French global network of broad band seismic stations [dataset]. Institut de physique du globe de Paris (IPGP), Universite de Paris. https://doi.org/10.18715/GEOSCOPE.G

IRIS DMC. (2011a). Data services products: Backprojection p-wave back-projection rupture imaging [dataset]. IRIS. https://doi.org/10.17611/DP/112180

IRISDMC. (2011b). Source time function for Mw 7.4 Windward Islands [dataset]. IRIS. https://doi.org/10.17611/DP/112180

Isacks, B., & Molnar, P. (1971). Distribution of stresses in the descending lithosphere from a global survey of focal-mechanism solutions of mantle earthquakes. *Reviews of Geophysics*, *9*(1), 103–174. https://doi.org/10.1029/RG009i001p00103

Jia, Z., Shen, Z., Zhan, Z., Li, C., Peng, Z., & Gurnis, M. (2020). The 2018 Fiji Mw 8.2 and 7.9 deep earthquakes: One doublet in two slabs. *Earth and Planetary Science Letters*, *531*, 115997. https://doi.org/10.1016/j.epsl.2019.115997

Kelemen, P., & Hirth, G. (2007). A periodic shear-heating mechanism for intermediate-depth earthquakes in the mantle. *Nature*, *446*(7137), 787–790. https://doi.org/10.1038/nature05717

Kirby, S., Hemingway, B. S., & Lee, R. (1990). Anomalous fracture and thermal behavior of hydrous minerals. In *The brittle-ductile transition in rocks* (pp. 119–126). American Geophysical Union. https://doi.org/10.1029/GM056p0119

Kiser, E., Ishii, M., Langmuir, C. H., Shearer, P. M., & Hirose, H. (2011). Insights into the mechanism of intermediate-depth earthquakes from source properties as imaged by back projection of multiple seismic phases. *Journal of Geophysical Research*, *116*(B6), B06310. https://doi.org/10.1029/2010JB007831

KNMI. (2006). Caribbean Netherlands seismic network [dataset]. Royal Netherlands Meteorological Institute (KNMI). https://doi.org/10.21944/dffa7a3f-7e3a-3b33-a436-516a01b6af3f

Knopoff, L., & Randall, M. J. (1970). The compensated linear-vector dipole: A possible mechanism for deep earthquakes. *Journal of Geophysical Research*, *75*(26), 4957–4963. https://doi.org/10.1029/JB075i026p04957

Laigle, M., Hirn, A., Sapin, M., Bécel, A., Charvis, P., Flueh, E., et al. (2013). Seismic structure and activity of the north-central Lesser Antilles subduction zone from an integrated approach: Similarities with the Tohoku Forearc. *Tectonophysics*, *603*, 1–20. https://doi.org/10.1016/j.tecto.2013.05.043

Laske, G., Masters, G., Ma, Z., & Pasyanos, M. (2013). Update on crust1.0 – A 1-degree global model of earth's crust. (pp. EGU2013–2658).

Li, J., Zheng, Y., Thomsen, L., Lapen, T., & Fang, X. (2018). Deep earthquakes in subducting slabs hosted in highly anisotropic rock fabric. *Nature Geoscience*, *11*(9), 696–700. https://doi.org/10.1038/s41561-018-0188-3

Libcomcat Developer Team. (2022). Libcomcat [software]. *USGS ANSS ComCat*. https://doi.org/10.5066/P91WN1UQ

Lindner, M., Rietbrock, A., Bie, L., Clouard, V., Collier, J., Goes, S. D. B., et al. (2019). Re-evaluation of the 2007 Mw7.4 intermediate-depth Martinique earthquake: Evidence for rupture on orthogonal faults. *AGU Fall Meeting Abstracts*, *2019*, T31D–0277.

Lindner, M., Rietbrock, A., Bie, L., Goes, S., Collier, J., Rychert, C., et al., the VOILA working group. (2022). Bayesian regional moment tensor from ocean bottom seismograms recorded in the Lesser Antilles: Implications for regional stress field. *Geophysical Journal International*, *233*(2), 1036–1054. https://doi.org/10.1093/gji/ggac494

MedNet Project Partner Institutions. (1990). Mediterranean very broadband seismographic network (MedNet) [dataset]. Istituto Nazionale di Geofisica e Vulcanologia (INGV). https://doi.org/10.13127/SD/fBBBtDtd6q

Müller, R. D., Zahirovic, S., Williams, S. E., Cannon, J., Seton, M., Bower, D. J., et al. (2019). A global plate model including lithospheric deformation along major rifts and orogens since the triassic. *Tectonics*, *38*(6), 1884–1907. https://doi.org/10.1029/2018TC005462

Persh, S. E., & Houston, H. (2004). Strongly depth-dependent aftershock production in deep earthquakes. *Bulletin of the Seismological Society of America*, *94*(5), 1808–1816. https://doi.org/10.1785/012003191

Pham, T.-S., & Tkalcic, H. (2021). Toward improving point-source moment-tensor inference by incorporating 1d earth model's uncertainty: Implications for the long valley caldera earthquakes. *Journal of Geophysical Research: Solid Earth*, *126*(11), e2021JB022477. https://doi.org/10.1029/2021JB022477

Poli, P., Prieto, G., Yu, C., Florez, M., Agurto-Detzel, H., Mikesell, T., et al. (2016). Complex rupture of the M6.3 2015 March 10 Bucaramanga earthquake: Evidence of strong weakening process. *Geophysical Journal International*, *205*(2), 988–994. https://doi.org/10.1093/gji/ggw065

Quinteros, J., Strollo, A., Evans, P. L., Hanka, W., Heinloo, A., Hemmleb, S., et al. (2021). The GEOFON program in 2020 [dataset]. *Seismological Research Letters*, *92*(3), 1610–1622. https://doi.org/10.1785/0220200415

Ranero, C. R., Villaseñor, A., Phipps Morgan, J., & Weinrebe, W. (2005). Relationship between bend-faulting at trenches and intermediate-depth seismicity. *Geochemistry, Geophysics, Geosystems*, *6*(12). https://doi.org/10.1029/2005GC000997

RESIF. (1995). Resif-rap French accelerometric network [dataset]. *RESIF – Reseau Sismologique et geodesique Francais*. https://doi.org/10.15778/RESIF.RA

Rodríguez-Cardozo, F., Hjörleifsdóttir, V., Jónsdóttir, K., Iglesias, A., Franco, S. I., Geirsson, H., et al. (2021). The 2014–2015 complex collapse of the Bárdarbunga caldera, Iceland, revealed by seismic moment tensors. *Journal of Volcanology and Geothermal Research*, *416*, 107275. https://doi.org/10.1016/j.jvolgeores.2021.107275

Rösler, B., Stein, S., & Spencer, B. (2023). When are non-double-couple components of seismic moment tensors reliable? *Seismica*, *2*(1). https://doi.org/10.26443/seismica.v2i1.241

Schlaphorst, D., Kendall, J.-M., Baptie, B., Latchman, J. L., & Tait, S. (2017). Gaps, tears and seismic anisotropy around the subducting slabs of the Antilles. *Tectonophysics*, *698*, 65–78. https://doi.org/10.1016/j.tecto.2017.01.002

Scripps Institution of Oceanography. (1986). Global seismograph network – IRIS/IDA [dataset]. *International Federation of Digital Seismograph Networks*. https://doi.org/10.7914/SN/II

Stein, S., F. Engeln, J., Wiens, D., Fujita, K., & C. Speed, R. (1982). Subduction seismicity and tectonics in the Lesser Antilles arc. *Journal of Geophysical Research*, *87*(B10), 8642–8664. https://doi.org/10.1029/JB087iB10p08642

University of Puerto Rico. (1986). Puerto Rico seismic network and Puerto Rico strong motion program [dataset]. *International Federation of Digital Seismograph Networks*. https://doi.org/10.7914/SN/PR

U.S. Geological Survey. (2022). Earthquake hazards program, 2017, advanced national seismic system (ANSS) comprehensive catalog of earthquake events and products: Various [dataset]. *USGS*. https://doi.org/10.5066/F7MS3QZH

van Driel, M., Krischer, L., Stähler, S. C., Hosseini, K., & Nissen-Meyer, T. (2015). Instaseis: Instant global seismograms based on a broadband waveform database [software]. *Solid Earth*, *6*(2), 701–717. https://doi.org/10.5194/se-6-701-2015

Vavryčuk, V., & Kühn, D. (2012). Moment tensor inversion of waveforms: A two-step time-frequency approach. *Geophysical Journal International*, *190*(3), 1761–1776. https://doi.org/10.1111/j.1365-246X.2012.05592.x

Wadati, K. (1928). Shallow and deep earthquakes. *Geophysical Magazine*, *1*, 162–202.

Wadge, G., & Shepherd, J. (1984). Segmentation of the Lesser Antilles subduction zone. *Earth and Planetary Science Letters*, *71*(2), 297–304. https://doi.org/10.1016/0012-821X(84)90094-3

Warren, L. M., Baluyut, E. C., Osburg, T., Lisac, K., & Kokkinen, S. (2015). Fault plane orientations of intermediate-depth and deep-focus earthquakes in the Japan-Kuril-Kamchatka subduction zone. *Journal of Geophysical Research: Solid Earth*, *120*(12), 8366–8382. https://doi.org/10.1002/2015JB012463

Zhan, Z., & Kanamori, H. (2016). Recurring large deep earthquakes in Hindu Kush driven by a sinking slab. *Geophysical Research Letters*, *43*(14), 7433–7441. https://doi.org/10.1002/2016GL069603